Stresses in Dolosse

Burcharth, Hans F.; Liu, Zhou; Howell, Gary L.; McDougal, W. G.

Published in:
Proceedings of the 22nd International Conference on Coastal Engineering : ICCE '90

Publication date:
1991

Document Version
Publisher's PDF, also known as Version of record

CHAPTER 106

Stresses in Dolosse

H.F. Burcharth[1] Liu Zhou[2] Gary L. Howell[3] W.G. McDougal[4]

Abstract

Failures of rubble mound breakwaters armoured with complex types of unreinforced concrete armour units are often due to breakage. This happens when the stresses exceed the material strength. Sufficient parametric studies of the stresses are not yet available to produce design diagrams for structural integrity.

The paper presents the results and the analyses of model tests with 200 kg and 200 g load-cell instrumented Dolosse. Static stresses and wave generated stresses were studied as well as model and scale effects. A preliminary design diagram for Dolosse is presented as well.

Introduction

Many of the recent dramatic failures of a number of large rubble mound breakwaters armoured with Dolosse and Tetrapods were caused by breakage of the concrete armour units. Breakage took place before the hydraulic stability of intact units in the armour layers expired. Thus there was an inbalance between the strength (structural integrity) of the units and the hydraulic stability (resistance to displacements) of the armour layer.

While the hydraulic stability can be roughly estimated by formulae and further evaluated in conventional hydraulic model tests, it is much more complicated to assess the structural integrity of the armour units. The increased research activity in this field has not yet resulted in generally applicable design diagrams or formulae by which the armour units can be designed as is the case for other civil engineering structural members.

For dealing with the problem the different types of loads on armour units and their origins might be listed as shown in Fig. 1.

[1]Prof. of Marine Civil Engineering, Aalborg University, Denmark.

[2]Ph.D., visiting researcher, Aalborg University, Denmark.

[3]Senior Research Engineer, Coastal Engineering Research Center, Waterways Experiment Station, U.S. Army Corps of Engineers, Vicksburg, Ms. USA.

[4]Ass. prof., Oregon State University, Corrallis, Oregon. Visiting prof. University of Aalborg, Denmark, 1987.

TYPES OF LOADS		ORIGIN OF LOADS	
STATIC		Weight of units	
		Prestressing due to: Settlement of underlayers Wedge effect and arching due to movements under dynamic loads	
DYNAMIC	Impact	Rocking/rolling of units	impacting solid bodies
		Missiles of broken units	
		Placing during construction	
	Pulsating	Gradually varying wave force including slamming	
		Earthquake	
ABRASION		Suspended material	
THERMAL		Stresses due to temperature differences during hardening processes	
		Freeze — thaw	
CHEMICAL		Corrosion of reinforcement	
		Sulfate reactions etc.	

Fig. 1. Types and origin of loads on armour units (from Burcharth, 1981).

It is characteristic for both static and dynamic load conditions that a deterministic calculation of the stresses in the units is practically impossible, mainly because of the stochastic nature of the wave loads, the complex shape of armour units and their random placements.

It is also characteristic of these stresses that they do not scale in the same way. Generally speaking the stresses due to non-impact loads increase linearly with the characteristic length of armour units, while impact-induced stress increases with the square root of the characteristic length. The relative importance of these stresses depends on the size and geometry of the units, their position on the slope and so on.

In this paper only static and pulsating stresses are considered.

Dolos static stress experiments in the dry (ramp tests)

Description of the experiment

With the purpose of studying the characteristics of static stresses in Dolosse and the related model and scale effects, a large field experiment programme was started in 1986 in Aalborg Hydraulic Laboratory (AHL) at Aalborg University. It includes comparative compaction experiments with 200 kg and 200 g Dolosse placed on ramps with various slope angles. The geometries of the Dolosse are given in Fig. 2.

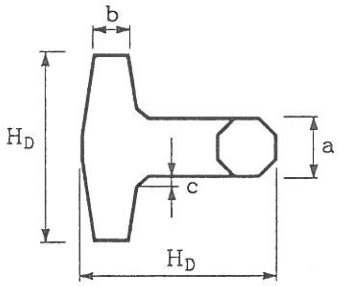

		app. 200 kg	app. 200 g
Height H_D	(cm)	80	8
Waist width a	(cm)	26	2.6
Head width b	(cm)	16	1.6
Height of fillet c	(cm)	4.0	0.46
Waist ratio		0.325	0.325

Fig. 2. Geometry of Dolosse.

200 kg strain-gauged Dolosse

Based on the structural consideration and practical experience, it is now generally accepted that Dolos fractures tend to occur in or near the shank-fluke interfaces. Consequently, two shank and two leg cross sections near the shank-fluke interfaces of 200 kg Dolosse were chosen as strain-gauged sections. Because the signals from the surface mounted strain gauges turned out to be too weak a load-cell solution was adopted. Four strain-gauge rossettes were mounted on the surfaces of steel tubes inserted as load cells in each of the chosen sections, cf. Fig. 3.

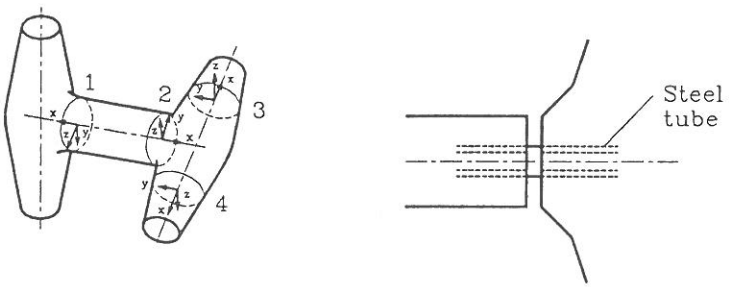

Fig. 3. Instrumented sections. 200 kg concrete Dolosse, Aalborg Hydraulic Laboratory (AHL).

The load cells allowed the following component forces/moments to be recorded, cf. Fig. 4, where the octahedal cross section is the correct one, and the circular cross section is an approximation (Burcharth et al., 1988).

The instrumentation made it possible to verify the relative importance of shear and axial forces.

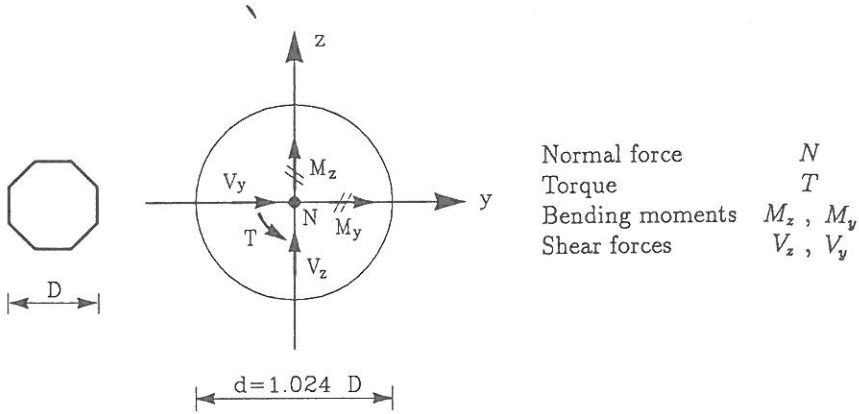

Fig. 4. Component forces/moments recorded in the instrumented sections.

200 g strain-gauged Dolosse

The applied units were developed by CERC and lent to the University of Aalborg (Markle, 1990). One shank cross section in the shank-fluke corner was strain-gauged to obtain two orthogonal bending moments and the torque. The stress contributions from axial and shear forces, which were believed to be of minor importance, were neglected.

The applied signal analysis, i.e. the transformation of the recorded load cell strains to armour unit stresses, is described in Burcharth et al., 1988. The first step in the signal analysis is to calculate the component forces/moments in the steel tube sections according to the recordings of strains. The next step is to transform these component forces into the stresses in the corresponding Dolos sections, and finally to calculate the maximum principal tensile stress, which is chosen as the critical parameter for the structural integrity of the armour units.

A large ramp (5 x 4 m) and a small ramp (0.5 x 0.4 m) with changeable slope angles were built. 72 Dolosse (200 kg or 200 g), including the instrumented ones, were randomly placed in two layers on the ramp. Every experiment involved the following 4 steps and corresponding recordings.

(i) Zeroing of strain gauges while the two instrumented Dolosse were in a specified position resting unloaded on ground.
(ii) Placement of the Dolosse on the ramp.
(iii) Vibration of the ramp.
(iv) Removal of Dolosse from the ramp and placement of the two instrumented Dolosse in the position described under (i).

Three pre-determined slopes were used: 1 : 0.9, 1 : 1.38 and 1 : 2. The instrumented Dolosse were 'randomly' placed at positions 1 and 2 in the bottom layer, as shown in Fig. 5.

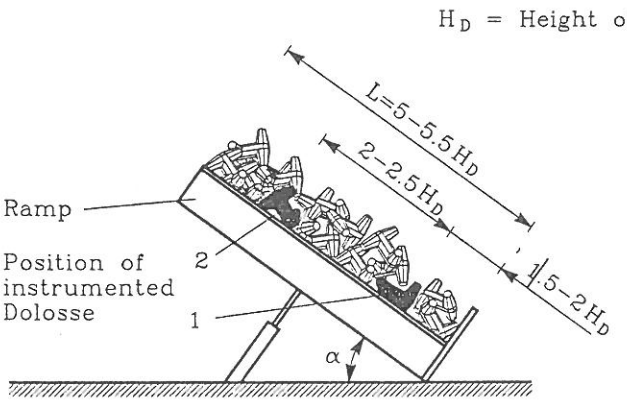

Fig. 5. Dolos compaction experiment set-up, Aalborg Hydraulic Laboratory (AHL).

Results from the static stress experiments (ramp tests)

Comparison of stresses in the shank and fluke cross sections

Because the small scale units cannot for practical reasons be instrumented in the fluke sections it is important to investigate if this implies a model error of any significance. From the tests with the 200 kg Dolosse it is clearly demonstrated in Table 1 that the max principal tensile stresses in the shank cross sections generally are bigger than those in the fluke cross sections.

Table 1. 200 kg Dolos compaction experiment results.

Group	1	2	3	4
Slope	1 : 0.9	1 : 1.38	1 : 1.38	1 : 2
Instrumented Dolos position	1	1	2	1
Average of σ_T in shank (MPa)	0.336	0.167	0.151	0.166
Average of σ_T in fluke (MPa)	0.181	0.157	0.088	0.12
No. of tests	28	40	36	20

σ_T denotes the max principal tensile stress in strain-gauged sections.

It is also seen that when dealing with results based on stresses only measured in the shank section it is necessary to compensate for the influence of fluke failures.

If it is assumed that the only relevant failure modes are fracture in the type of sections shown in Fig. 3, i.e. 2 shank sections and 4 fluke sections, then it is possible to calculate the probability of failure for the Dolosse, P_{Dolos}, from the probability of failure in the fluke section, P_{fluke}, and the probability of failure in the shank section, P_{shank} if the correlations between the various failure modes are known. If the Dolos is modelled as a series system, consisting of n elements $i = 1, 2, \ldots, n$, i.e. the failure of the Dolos takes place when any one of the element fails, then the probability of failure for the Dolos can be estimated as

$$P_{Dolos}(\sigma_T) \simeq 1 - \Phi_n(\bar{\beta}; \bar{\bar{\rho}})$$

where $\bar{\beta} = (\beta_1, \ldots, \beta_n)$ and $\beta_i(\sigma_T) = -\Phi^{-1}(P_i(\sigma_T))$ is the generalized reliability index corresponding to failure mode i. Each failure mode is approximated by a linear failure function in independent standard normal variables.

$\bar{\bar{\rho}} = [\rho_{ij}]$ is the correlation matrix for the linear failure functions.

$\Phi_n = n$-dimensional standardized normal distribution.

Generally calculation of $\Phi_n(\bar{\beta}; \bar{\bar{\rho}})$ for $n \geq 3$ cannot be performed exactly but the Hohenbichler approximation can be used (Thoft-Christensen et al. 1986). $n = 6$ in the proposed model for a Dolos. Alternatively reliability bounds can be calculated. A simple lower bound is the maximum probability of failure of any element, in this case corresponding to P_{shank}. This lower bound corresponds to full correlation between all elements, i.e. $\rho_{ij} = 1$ for all i and j. A simple upper bound can be found by assuming non-correlated elements in which case we get

$$P_{Dolos}(\sigma_T) = 1 - (1 - P_{shank}(\sigma_T))^2 (1 - P_{fluke}(\sigma_T))^4$$

The assumption of non-correlated elements gives the highest possible probability of failure. More narrow bounds can be found if the correlations are known. The simple lower and upper bounds are shown in Fig. 6 together with an estimate of the real failure probability based on a Hohenbichler approximation. The high stress levels shown in the Figure are due to the inclusion of test results from the very steep 1 : 0.9 slope.

Influence of Dolos position and slope angle

The results in Table 1 show as expected that the dolosse situated in lower positions of the bottom layer have greater stresses than those situated in the higher positions, and the dolos stress increases with steeper slopes, other conditions being equal.

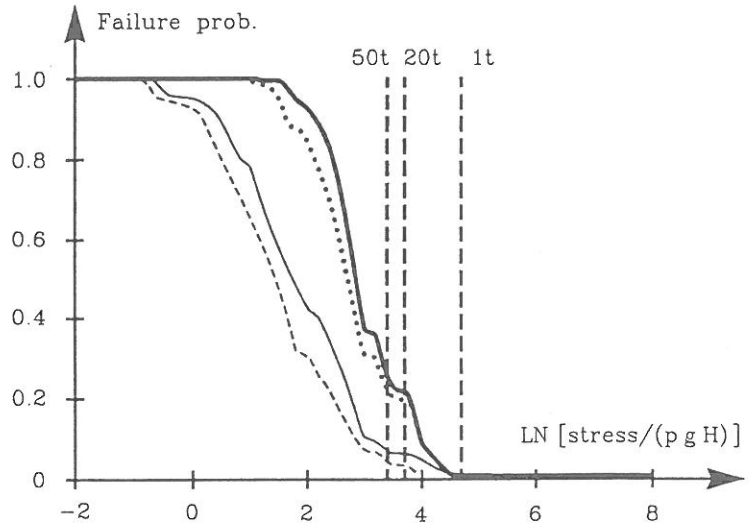

Slope : 1 in 0.9, 1,38, 2. Instrumented Dolos position 1, 2
——— : Simple upper bound of Dolos failure probability
····· : App. failure probability of Dolos
——— : Failure probability of shank. (Simple lower bound of Dolos failure probability)
----- : Failure probability of fluke
– – – : Structural limitation of Dolosse with weight 1, 20 and 50 t, waist ratio 0.32, density 2300 kg/m^3 and strength 3.5 MPa

Fig. 6. Failure probability of Dolosse based on recorded static stresses in ramp tests in the dry, AHL experiments.

The stress distribution

The measured maximum principal tensile stresses σ_T followed the log-normal distribution both in the shank and the fluke cross sections. The density function is given by

$$f(\ln \sigma_T) = \frac{1}{\sigma\sqrt{2\pi}} e^{-\frac{1}{2}\left(\frac{\ln \sigma_T - \mu}{\sigma}\right)^2}$$

$$\mu = \frac{1}{N}\sum_{i=1}^{N} \ln(\sigma_T)_i \qquad \sigma^2 = \frac{1}{N-1}\sum_{i=1}^{N} (\ln(\sigma_T)_i - \mu)^2$$

where μ and σ are average and standard deviation respectively.

The conclusion on stress distribution is consistent with results from small scale tests conducted by D. Turke, Canada (private communication), see also Anglin et al., 1990.

Stress contribution from shear and axial forces

In small scale tests it is difficult or even impossible to mount a sufficient number of strain gauges inside small Dolosse to determine all component forces/moments in a cross section. Generally the stress contributions from axial and shear forces are regarded of minor importance. To check this hypothesis the distribution of $(\sigma_T - \sigma'_T/\sigma_T)$, where σ'_T represents the corresponding maximum principal tensile stress without axial and shear forces, is plotted in Fig. 7. The results are from the fully instrumented 200 kg Dolosse and represent only the conditions in the instrumented shank sections. From this Figure the following can be concluded:

(i) the bigger σ_T, the smaller $(\sigma_T - \sigma'_T/\sigma_T)$, i.e. reduced influence from axial and shear forces.

(ii) The negligence of axial and shear forces most likely results in overestimation of the max principal tensile stress. In other words, it is on the safe side.

Slope : 1 in 0.9, 1.38, 2. Instrumented Dolos position 1, 2
- - - : Fracture limitation of concrete Dolosse (density 2300 kg/m^3, tensile strength 3.5 MPa)
— · — : Exceedence probability

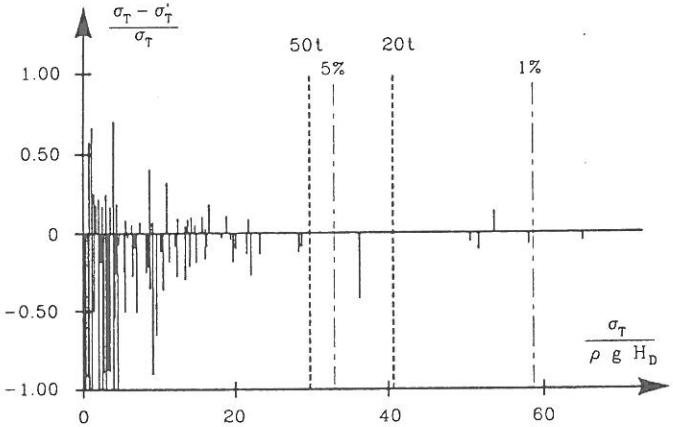

Figure 7. Example of stress contribution from axial and shear forces. Tests with 200 kg Dolosse, Aalborg Hydraulic Laboratory (AHL) experiments.

Comparison of static stress distributions in large and small scale experiments including verification of the scaling law

Fig. 8 shows the exceedence probability of the dimensionless maximum principal tensile stress in 200 kg and 200 g concrete Dolosse in the compaction experiment.

It is consistent (especially for high stress levels), with the theoretical scaling law $\lambda_\sigma = \lambda_\rho \lambda_L$, where $\lambda_\sigma, \lambda_L$ and λ_ρ are scaling factors for stress, length and density, respectively.

Slope : 1 in 0.9, 1.38, 2. Instrumented Dolos position: 1 and 2.
- - - : Fracture limitation of concrete Dolosse (density 2300 kg/m^3, tensile strength 3.5 MPa)
——— : 200 g concrete Dolos (without shear and axial forces)
——— : 200 kg concrete Dolos (without shear and axial forces)

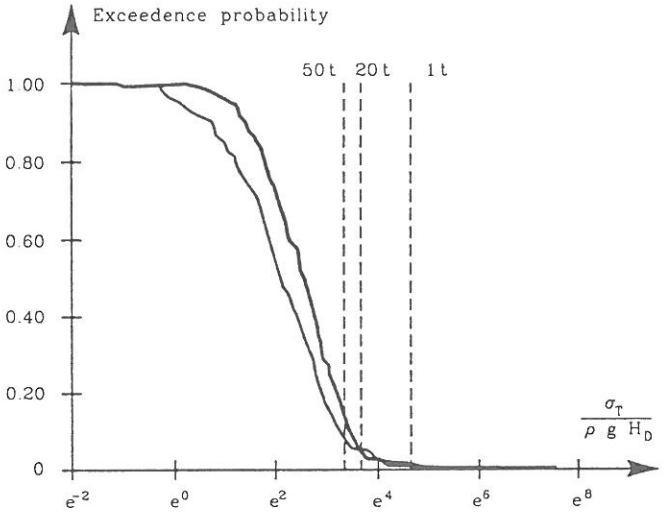

Figure 8. Comparison of stress distributions in shank cross sections of 200 kg and 200 g concrete Dolosse. Influence from shear and axial forces are neglected. AHL experiments.

Influence of compaction and surface roughness

Comparative tests with smooth (polyester) and rough (concrete) Dolosse revealed that the amount of compaction (settlement) and the surface roughness influenced the stresses significantly. The effects should be consideres in the model test analysis.

Hydraulic flume tests

The object of the flume tests at AHL is to study the armour unit stresses as functions of the structural and the sea state parameters.

Although a comprehensive parametric study has not yet been completed, enough tests have been made to present some conclusions related to a range of problems. The set-up and procedure for the tests are coordinated with tests at CERC, Vicksburg, in order to establish a more complete parametric study.

Model test set-up and description of the experiments

All tests were conducted in a 1.2 m wide and 1.5 m deep flume with the model situated app. 17 m from the wave paddle, Fig. 9. The flume was divided into two parts with width of 0.75 m and 0.45 m, respectively. The breakwater model was placed in the 0.75 m wide part of the flume at the top end of a 1 : 20 foreshore slope. The water depth at the toe of the breakwater was 23 cm. The 0.45 m wide part of the flume was fitted with an effective non-reflecting array of perforated metal sheets. Fig. 9 also shows the cross section of the breakwater.

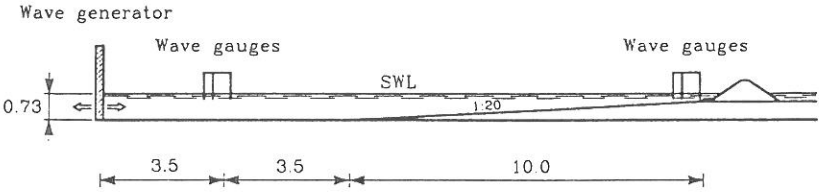

Set-up of the wave flume

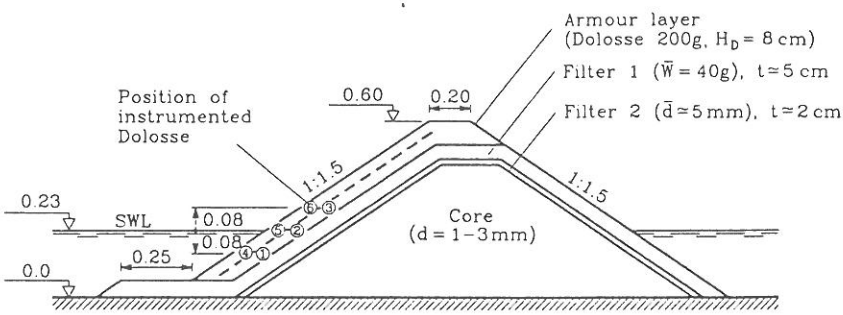

Cross section of the breakwater

Measures and levels in meter

Fig. 9. Set-up of the wave flume and the cross section of the breakwater. Aalborg Hydraulic Laboratory (AHL) experiments.

To compensate for reflected waves two arrays of three wave gauges were installed. The incident wave spectrum was calculated by the least square method presented by Mansard et al., 1980.

The irregular waves were generated by a piston type paddle according to the five parameter JONSWAP spectrum with the peak enhancement coefficient being 4.

Table 2 lists the characteristics of the applied waves propagating towards the breakwater at the paddle and at the toe of the breakwater. L_p is wave length

corresponding to the spectral peak period and $\zeta = T_p \left(\frac{2\pi}{gH_{m0}}\right)^{0.5} tan\alpha$.

Table 2. H_{m0} and T_p at the wave paddle and at the toe of the structure.

H^p_{m0}	at the paddle	(cm)	5	10	15
T_p	at the paddle	(sec)	1.5	2	2
H^p_{m0}/L_p	at the paddle		0.016	0.022	0.032
H^t_{m0}	at the toe	(cm)	5.7	11.8	17.9
T_p	at the toe	(sec)	1.5	2	2
ζ	with H^p_{m0} and $tan\alpha = \frac{1}{20}$		0.27	0.25	0.21
ζ	with H^t_{m0} and $tan\alpha = \frac{1}{1.5}$		3.3	3.1	2.5

Definition of peaks of static plus pulsating stresses

In the statistical analyses of the stress peaks presented in the paper a definition of the peaks by zero down crossing identification has been adopted, Fig. 10. This definition is applied due to the fact that static and pulsating stresses scale the same way.

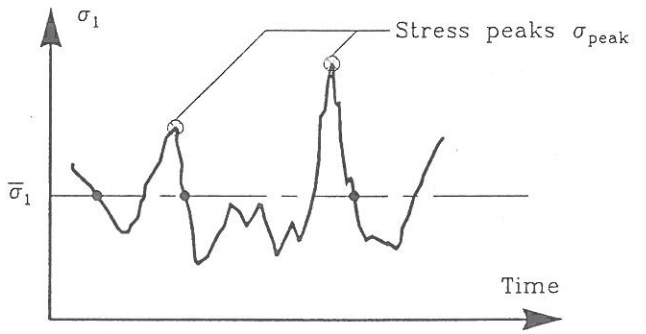

Figure 10. Definition of peaks of stress in time series.

Results from the flume tests

Distribution of static stresses

The distribution of the static stresses which are defined as the average of the Dolos stresses before and after wave attacks is shown in Fig. 11. As is seen the distribution closely follows the log-normal distribution as also found from the ramp tests.

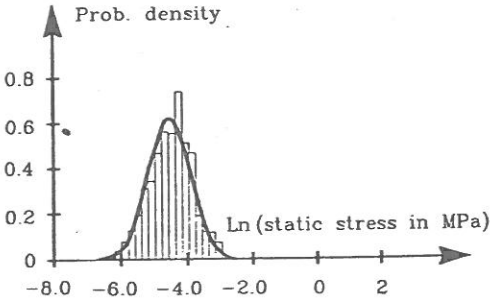

Figure 11. Distribution of static stresses in flume tests with 200 g Dolosse as recorded in one shank cross section.

Distribution of stress peaks for static plus pulsating loads

Fig. 12 shows for three different sea states the stress distributions obtained from the flume tests with 200 g Dolosse only instrumented in one shank cross section. Results are for 6 positions of Dolosse within the area between levels SWL ± app. 1.5 times the Dolos height.

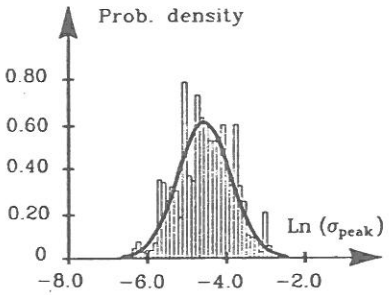

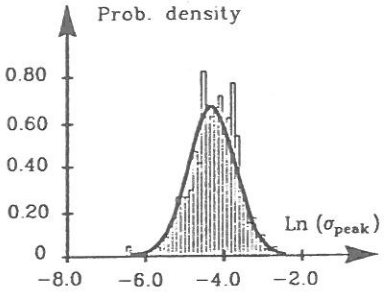

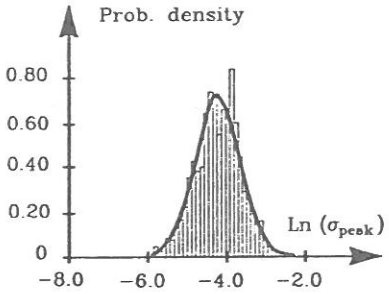

	a	b	c
H^p_{m0} (cm)	5	10	15
Number of stress peaks	19558	16320	17785
Average of $Ln(\sigma_p)$	−4.56	−4.29	−4.21
Standard dev. of $Ln(\sigma_p)$	0.66	0.59	0.55

Figure 12. Distribution of peaks of static and pulsating stresses (in MPa).

It is seen that the mean values (mean of *ln*) increase with the wave height, but at the same time the standard deviation decreases. Consequently, the stress corresponding to higher exceedence probability levels are found to be almost invariant to the wave height for waves higher than a certain level, cf. also Fig. 12. This tendency can also be seen in model test results with Tetrapods, Bürger et al., 1990.

Preliminary design chart

Fig. 13 is an example of a preliminary design chart. *Note that the static stresses (corresponding to zero wave height) are large compared with the total stresses under wave action.*

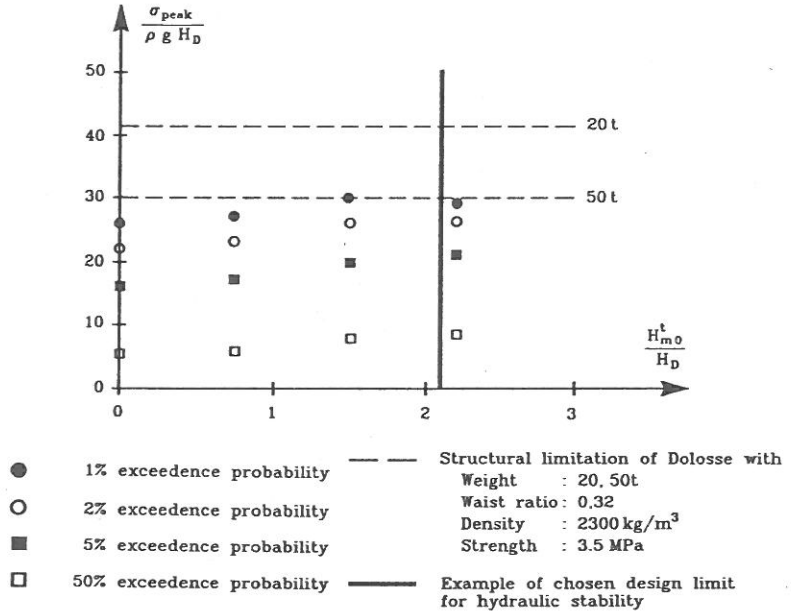

Figure 13. Preliminary design chart for Dolos with waist ratio 0.32. The design chart covers the area between levels SWL ± app. 1.5 times the Dolos height. The exceedence probabilities are obtained from the fitted log-normal distribution of peaks of static and pulsating stresses. Impact stress, fatigue, failure contribution from flukes and surface roughness correction are not included.

Within the tested range it was found that the wave generated pulsating stresses, in terms of the average of the significant stress wave height, increase almost linearly with the significant wave height.

Acknowledgement

The valuable asistance of Dr. L. Pilegaard-Hansen, Institute of Building Technology, University of Aalborg, in the early phase of the ramp tests is very much appreciated. The work reported here was part of a cooperative effort between the Crescent City Prototype Dolosse Study of the Coastal Engineering Research Center and the University of Aalborg. Permission to publish this paper has been granted by the US Army Corps of Engineers, Office, Chief of Engineers.

References

Anglin, C.D., R.D. Scott, D.I. Turcke, M.A. Turcke (1990): *The development of structural design criteria for breakwater armour units.* Proc. Seminar Stresses in Concrete Armor Units, ASCE, Vicksburg, U.S.A., 1990.

Burcharth, H.F. (1981) : *Full-scale dynamic testing of dolosse to destruction.* Coastal Engineering, Vol.4, 1981.

Burcharth, H.F. and Gary Howell (1988): *On methods of establishing design diagrams for structural integrity of slender complex types of breakwater armour units.* Seminaire International Entretien des Infrastructures Maritimes. Casablanca, Marocco, 1988.

Burcharth, H.F. and Liu Zhou (1990): *A general discussion of problems related to the determination of concrete armour unit stresses including specific results related to static and dynamic stresses in Dolosse.* Proc. Seminar Stresses in Concrete Armor Units, ASCE, Vicksburg, U.S.A., 1990.

Bürger, H. Oumeraci, H.W. Partenscky (1990): *Impact Strain Investigations on Tetrapods: Results of Dry and Hydraulic Tests.* Proc. Seminar Stresses in Concrete Armor Units, ASCE, Vicksburg, U.S.A., 1990.

Mansard, E.P.D., E.R. Funke (1980): *The measurements of incident and reflected spectra using a Least Squares Method.* Proceeding of the 17th International Conference on Coastal Engineering, Sydney, Australia, March 1980.

Markle, D.G. (1990): *Crescent City Instrumented Model Dolos Study.* Proc. Seminar Stresses in Concrete Armor Units, ASCE, Vicksburg, U.S.A., 1990